JOURNAL OF APPLIED ELECTROCHEMISTRY 15 (1985) 557–566

*Mass and momentum transfer enhancement due to electrogenerated gas bubbles**

F. GIRON, G. VALENTIN, M. LEBOUCHE‡, A. STORCK

Laboratoire des Sciences du Génie Chimique, CNRS-ENSIC, 1 rue Grandville, 54042 Nancy Cedex, France

Received 27 November 1984

The effect of electrogenerated gas bubbles with simultaneous bulk liquid flow on the mass and momentum transfer at a wall of an electrolytic cell is experimentally determined. The local mass transfer coefficient and electrolyte shear stress are obtained using two types of microelectrodes imbedded in the channel wall. The influence of the most important parameters (electrolyte velocity, position along the wall, gas electrogeneration rate) on the transfer enhancement is studied and an analogy between mass and momentum transfer in the presence of bubbles is clearly demonstrated from the experimental results. The comparison with classical correlations, valid for systems involving natural turbulence, shows the higher energetic efficiency of devices where the turbulence is artificially generated by electrolytic gas bubbles.

Nomenclature

A	constant parameter in Equation 3
$\bar{C}$	time averaged value of the concentration of a reacting species
C_0	molar concentration in the bulk of the solution
d	microelectrode diameter
d_e	hydraulic equivalent diameter
D	molecular diffusion coefficient
D_t	turbulent diffusivity of mass transfer
$f/2$	friction factor, $= \tau/\rho\bar{v}^2$
h	channel thickness
I_g	electrogeneration rate
i_g	electrogeneration current density
i_L	limiting current density on a microelectrode imbedded in the conducting wall
i'_L	limiting current density on a microelectrode imbedded in the inert wall
k_d	local mass transfer coefficient
k'	local mass transfer coefficient on a microelectrode in the non-conducting wall
N_M	specific mass flux near an interface
Re	Reynolds number, $= (\bar{v}d_e)/\nu$
s	velocity gradient, $= (\partial\bar{v}_x/\partial y)_{y=0}$
s^+	dimensionless velocity gradient, $= sd^2/D$
Sc	Schmidt number, $= \nu/D$
Sh	Sherwood number, $= (k_d x)/D$
St	Stanton number, $= k_d/\bar{v}$
$\bar{v}, \bar{v}_x$	electrolyte velocity
v^*	friction velocity, $= (\tau/\rho)^{1/2}$
v^+	normalized velocity, $= \bar{v}_x/v^*$
x	axial coordinate
y	coordinate perpendicular to the wall
y^+	dimensionless length $= (yv^*)/\nu$

Greek letters

α	parameter defined in Equation 8
δ	boundary layer thickness
δ^+	dimensionless form of δ, $= \delta(s/\nu)^{1/2}$
τ, τ_x	electrolyte shear stress
μ	dynamic viscosity
ν	kinematic viscosity
ν_t	momentum transfer diffusivity
ρ	specific gravity
σ^2	variance of the fluctuations of i_L or i'_L

* Paper presented at the International Meeting on Electrolytic Bubbles organized by the Electrochemical Technology Group of the Society of Chemical Industry, and held at Imperial College, London, 13–14 September 1984.
‡ Laboratoire d'Energétique et de Mécanique Théoriques et Appliquées CNRS (ERA 893), 2 rue de la Citadelle 54042 Nancy Cedex, France.

0021–891X/85 $03.00 + .12

1. Introduction

It is well known that mass transfer rates between a flowing electrolyte and an electrode (plate or porous) can be substantially increased by the turbulence induced at the level of the diffusional boundary layer near the electrode. In practical applications, two situations may be encountered:

(a) Artificial bubbles generated by another upstream counter electrode or present together with a liquid (as in a classical gas–liquid–solid absorption apparatus) disturb the boundary layer near the downstream working electrode [1–3].

(b) Bubbles (frequently H_2 or O_2) are electrogenerated inside the layer leading to a sharp increase in the mass transfer coefficient between the liquid and the electrode.

This second point has been the subject of numerous studies and several models have been proposed for describing the mechanism of mass transfer enhancement through gas evolution [4–9]. In the *penetration model*, Ibl and Venczel [4] have suggested that the detachment of a bubble from the electrode creates an empty space, which is filled by fresh solution. During the waiting time, mass transfer is governed predominantly by non-steady diffusion in a quiescent liquid. A variation of Ibl's model was presented by Rousar and Cezner [5]. The *microconvection model* presented by Stephan and Vogt [6] considers that the growing bubble induces a liquid flow past the electrode surface and disregards the diffusion in the quiescent liquid. Lastly, in the *hydrodynamic model* proposed by Janssen [7–9], it was supposed that the main phenomenon governing the mass transfer rate is the macroscopic motion of fluid induced by the ascending bubbles.

The main aim of this paper is to present experimental data of mass transfer and to clarify the connecting mechanism between mass and momentum transfer in systems involving simultaneous gas evolution and forced convection of the electrolyte.

By means of microelectrodes inserted into the working electrode, it has been possible to determine:

(a) the spatial distribution of the mass transfer coefficient k_d along the vertical plane by means of the diffusion controlled electrochemical reduction of ferricyanide ions;

(b) the distribution of the electrolyte velocity gradient $s = (\partial v_x/\partial y)_{y=0}$ at the surface (momentum transfer parameter);

(c) the intensity of turbulence by measuring the variance σ^2 of the fluctuations of the limiting current density.

The influence of the most important parameters (electrolyte flowrate $\bar{v}$ varied between 0.2 and 2 cm s^{-1}, electrogeneration rate i_g varied between 0 and 500 A m^{-2}) has been studied experimentally. Furthermore the relation between mass and momentum transfer was deduced from the experimental results and compared to well-known correlations based on the analogy between mass and momentum transfer in natural turbulence.

2. Experimental details

2.1. *Electrolytic cell*

The experimental circuit is schematically represented in Fig. 1; its main component is the vertical cell composed of a rectangular channel divided into two compartments by means of an asbestos diaphragm. The two nickel electrodes (length: 0.4 m; width 0.1 m; area 400 cm^2) are separated by a distance of 0.05 m. The flowing electrolytes are an aqueous solution of potassium ferri- and ferrocyanide (respectively 5×10^{-3} M and 10^{-2} M) in potassium hydroxyde (1 M). The temperature is controlled at 20 ± 1° C and the electrolyte flowrates are measured with two rotameters. At the outlet of the cell, two gas–liquid separators allow recycling of the pure electrolyte to the cell inlet. An amperostat is connected to the anodic and cathodic plates and fixes the desired overall current density in the cell.

2.2. *The microelectrodes*

Two types of nickel microelectrode have been used:

(a) a series of microelectrodes (diameter 0.8 mm) inserted into the cathodic plate and electrically insulated from the working electrode (Ni plate) by a small film of 'Araldite'. By a classical potentiostatic circuit, these microelectrodes are maintained at a potential corresponding to the limiting current density i_L for the reduction of ferricyanide ions $Fe(CN)_6^{3-}$. From the experimental determination of i_L at a given position along the

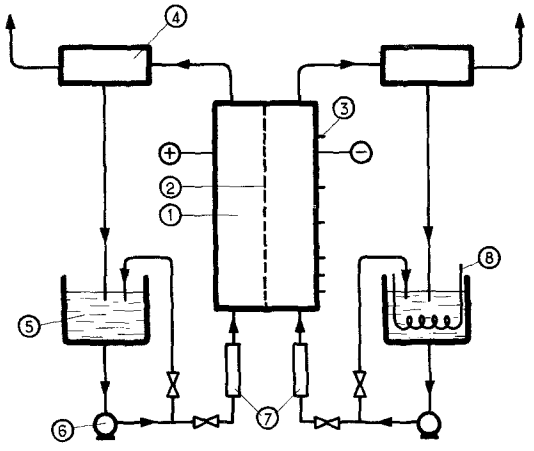

Fig. 1. Schematic view of the apparatus. 1-cell, 2-diaphragm, 3-microelectrode, 4-gas–liquid separator, 5-storage tank, 6-pump, 7-liquid rotameters, 8-cooling element.

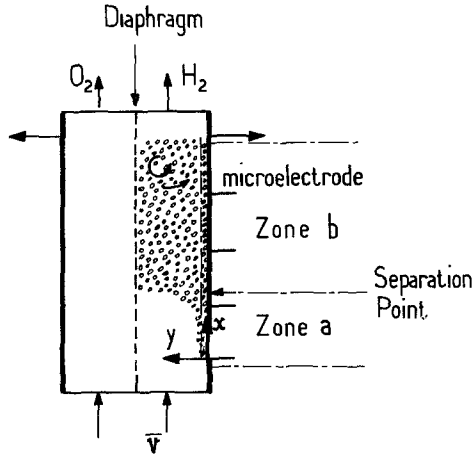

Fig. 2. Schematic representation of the gas–liquid flow inside the cathodic compartment.

plate, it is possible to deduce the local mass transfer coefficient k_d between the liquid and the wall.

(b) a series of microelectrodes (diameter 0.5 mm) inserted into a vertical non-conducting layer (width 2 mm), itself located in the middle of the cathodic plate.

The measurement of the limiting current density i'_L and of the corresponding mass transfer coefficient k' leads to the local value of the velocity gradient $s = (\partial v_x/\partial y)_{y=0}$ through the relation:

$$k' = 0.807 \frac{D^{2/3} s^{1/3}}{d^{1/3}} \qquad (1)$$

where D is the diffusion coefficient of the reacting species ($Fe(CN)_6^{3-}$) and d the microelectrode diameter. For a Newtonian fluid, the fluid shear stress $\tau = \mu s$ may also be obtained.

These two techniques (microelectrodes in conducting or insulated plates) have already been presented in previous papers [10–12]. The validity of the measurements of s by electrochemical determination in a two-phase flow system will be discussed in section 3.4.

3. Results

3.1. *Visual observations*

The visual observation of the electrolyte flow inside the cathodic compartment shows the existence of two zones, when the gas electrogeneration rate i_g is sufficient (cf. Fig. 2):

the first zone (a) located upstream characterized by a rapid ascending bubble train near the electrode;

the second eddy zone (b), in which recirculation of a gas liquid dispersion occurs in the whole channel thickness. The separation point between these two zones is very well defined and its position depends simultaneously on $\bar{v}$ and i_g. Such an observation has been already mentioned by other authors [13].

3.2. *Mass transfer results*

The three Figs. 3 to 5 summarize most of the mass transfer results (k_d) and show the influence of the position x along the plate, the electrogeneration rate I_g and the electrolyte velocity $\bar{v}$. Fig. 3 shows a typical curve for the spatial distribution of k_d. At a given position x, the thickness δ of the diffusion boundary layer decreases very sharply at first as the gas discharge rate I_g increases and then

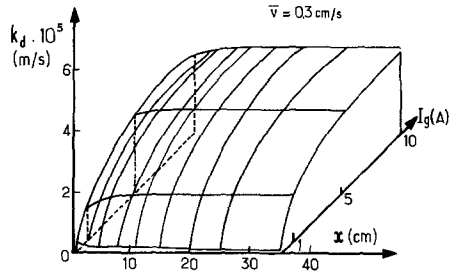

Fig. 3. Influence of the position x and electrogeneration rate I_g on the local mass transfer coefficient k_d.

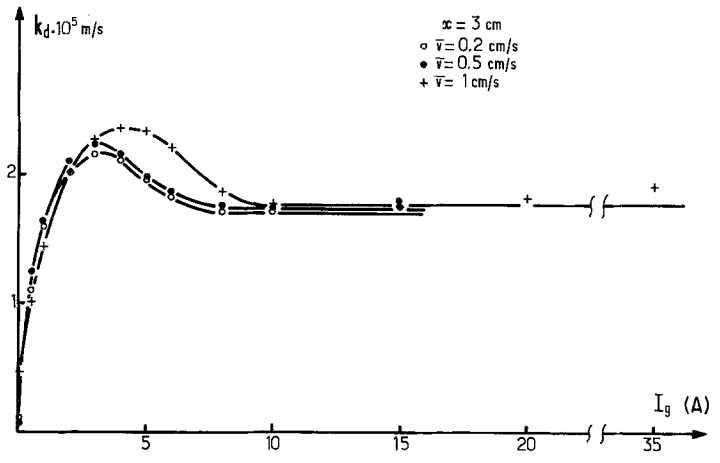

Fig. 4. Influence of I_g on k_d for three electrolyte velocities.

a stabilization occurs for $I_g > 3$A (i.e. $i_g > 75$ A m^{-2}); the relative increase of k_d can be as high as 3000% compared to the pure electrolyte (when $i_g = 0$). For a given value of I_g, the effect of x is such that a rapid increase of k_d is observed in the first centimetres of the wall and then it remains constant.

A more precise determination of the effect of i_g is shown in Fig. 4 for three different velocities $\bar{v}$. k_d, which increases very sharply at first, reaches a maximum and then decreases slowly to a limiting value in the range of variations studied ($I_g < 35$ A or $i_g < 870$ A m^{-2}). These results and more precisely the existence of a plateau for the mass transfer coefficient are in good agreement with those of Elsner and Marchiano [14], who used segmented electrodes for determining the effect of a train of bubbles generated upstream of the test electrode.

It should be mentioned also from the results of Figs. 4 and 5 that the effect of $\bar{v}$ is very weak (for $\bar{v} < 2$ cm s^{-1}). Therefore the marked increase of k_d is mainly determined by the turbulence generated by the gas bubbles (H_2 here) and not by the macroscopic convective movement of the liquid. Fig. 6 presents the variation of the diffusion boundary layer δ with i_g obtained in this study and in other works dealing with vertical walls, where electrogeneration of H_2 occurs. The same order of magnitude is observed, though the operating conditions are quite different, because the microelectrodes do not generate gas bubbles in our case.

3.3. *Analysis of the fluctuations*

The variance σ^2 of the fluctuations of the limiting current density i_L (proportional to k_d) on a given microelectrode is shown in Fig. 7 for $x = 3$ cm and $x = 20$ cm. The point $x = 3$ cm is always located in zone (a) whatever i_g, whereas $x = 20$ cm is in zone (a) or (b) depending on the value of i_g.

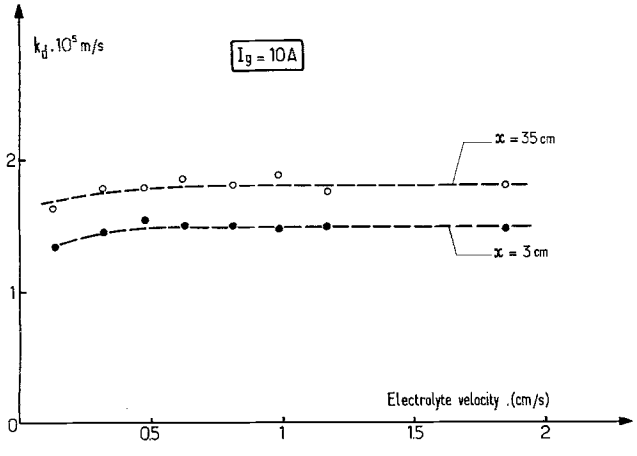

Fig. 5. Influence of the electrolyte velocity on k_d at two positions along the wall. I_g = 10A.

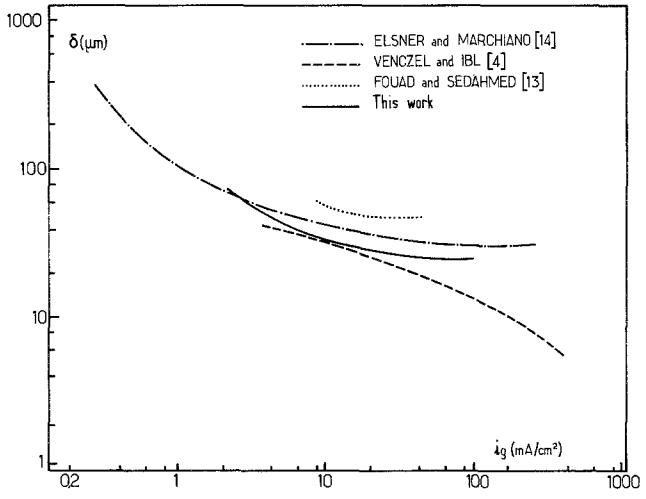

Fig. 6. Variations of the boundary layer thickness δ with the electrogeneration rate current density i_g. Comparison with other works.

In the zone composed of rapidly ascending bubbles, the values of σ^2 are very low ($\sigma^2 < 50 \times 10^{-5}$ A^2), and the variance shows a maximum for a current density i_g of the same order of magnitude as the one corresponding to the maximum of k_d (cf. Fig. 4). For the microelectrode in the upper part of the wall ($x = 20$ cm), σ^2 shows higher values and from the separation point characterized by the recirculation ($I_g > 6$ A), the slope of the increase of σ^2 with I_g is much higher. It is interesting to compare this effect to the one mentioned in Fig. 3 (for $x = 20$ cm). There is no direct relation between σ^2 (indicative of the turbulence intensity at the microelectrode) and k_d. Indeed, for $I_g > 6$ A, the mass transfer coefficient remains constant whereas σ^2 increases practically linearly with I_g. So the higher turbulence induced by the eddies of the gas–liquid dispersion has no measurable effect on k_d. In fact, and this could be an explanation for the constancy of k_d, bubbles present inside the diffusion layer can generate turbulent diffusion which has a favourable effect on the mean value of k_d. On the other hand, external bubbles may induce very high fluctuations of k_d by disturbing the outside part of this layer but without leading to an increase of the turbulent diffusivity.

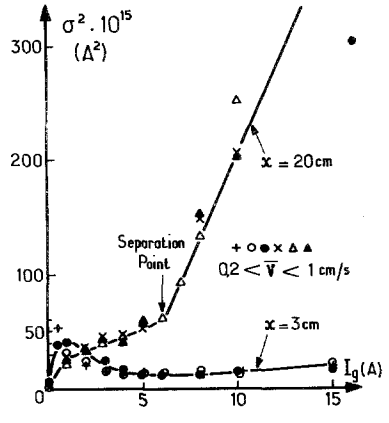

Fig. 7. Experimental variations of the variance σ^2 characterizing the fluctuations of the mass transfer limiting current density with I_g: influence of the position x.

3.4. *Momentum transfer results*

Fig. 8 gives the variations of the velocity gradient s with the electrogeneration rate I_g, at two positions along the electrode and for a given electrolyte velocity $\bar{v}$.

For $I_g = 0$ (no gas bubble), s shows low values and increases quite rapidly when the gas discharge occurs. The trends observed are very similar to those of k_d with I_g; however, the plateau is less

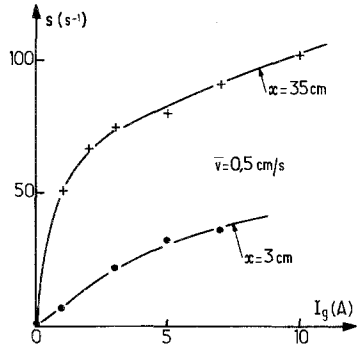

Fig. 8. Variations of the velocity gradient s with I_g at two positions.

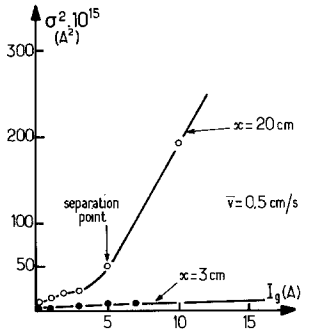

Fig. 9. Experimental variations of the variance σ^2 characterizing the fluctuations of the limiting current density i'_L on a microelectrode imbedded in the non-conducting layer.

pronounced. The analogy between mass and momentum transfer is therefore clearly demonstrated and also verified by considering the variance σ^2 of the fluctuations of the limiting current density i'_L at the microelectrodes inserted in the vertical non-conducting layer (results of Fig. 9 compared to those of Fig. 7). Consequently the favourable enhancement of k_d through gas discharge is very strongly related to the increase of the electrolyte shear stress, $\tau = \mu s$, at the wall.

At this point it is appropriate to discuss the validity of the measurement of s using the electrochemical technique since up to the present its validity has only been proven for single phase flow and certain particular cases in gas–liquid flow [15]. For a single phase flow, Fig. 10a represents the concentration distribution of the reacting species near a circular microelectrode with a diameter d imbedded in an inert wall. Fig. 10b gives, in an adimensional representation, the variation of the boundary layer thickness $\delta^+ = \delta(s/\nu)^{1/2}$ with the velocity gradient $s^+ = sd^2/D$ (δ corresponds to the value of y where $C/C_0 = 0.9$). As a first approximation, the measurement of s in a gas–liquid flow will be correct if no bubbles are present in the zone δ near the microelectrode. For our experimental conditions ($d = 0.5$ mm; $D = 7.65 \times 10^{-10}$ m^2 s^{-1} and $\nu = 0.94 \times 10^{-6}$ m^2 s^{-1}), Table 1 reports the thickness δ for different values of s. δ decreases when s increases and for $s > 50\,s^{-1}$ the boundary layer thickness is smaller than 70 μm. It seems reasonable to assume that no bubble is present in this thickness (for the vertical non conducting layer) and that the hydrodynamic conditions prevailing in this region are not very different from those existing at the level of the conducting wall, where gas discharge occurs. This is particularly true given the small width (2 mm) of the inert layer.

4. Relation between mass and momentum transfer

The qualitative analogy observed previously between both transfer mechanisms suggests the possibility of correlating quantitatively informations on both k_d, mass transfer coefficient and k', momentum transfer parameter, cf. Equation 1. From the experimental results obtained in this study, Fig. 11 presents this relation between k_d and k', on a logarithmic scale, in both the pure liquid ($I_g = 0$) and in the presence of electrogenerated gas bubbles.

The following conclusions may be derived.

1. For $I_g = 0$ (no bubble), the experimental results (k_d versus k') are in good agreement with the theoretical analysis of mass and momentum transfer in a parallelepipedic channel (laminar flow regime). Indeed [16], the velocity gradient s is given by:

$$s = \left(\frac{\partial v_x}{\partial y}\right)_{y=0} = \frac{6\bar{v}}{h} \qquad (2)$$

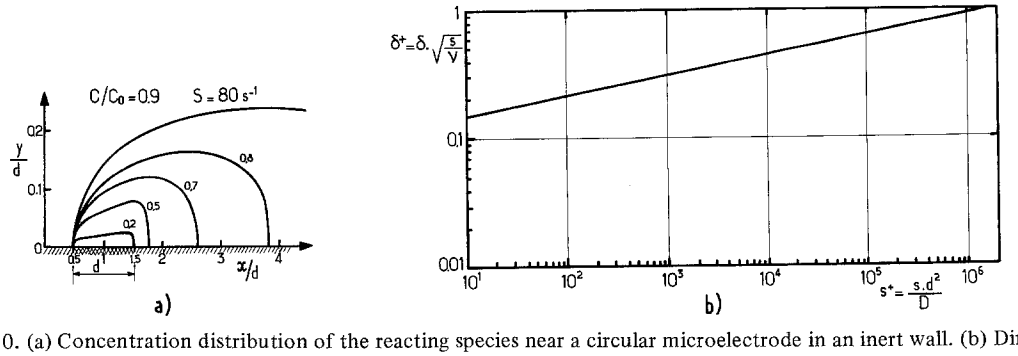

Fig. 10. (a) Concentration distribution of the reacting species near a circular microelectrode in an inert wall. (b) Dimensionless thickness δ^+ of the diffusion boundary layer.

Table 1.

$s(s^{-1})$	s^+	δ^+	$\delta(\mu m)$
10	3268	0.38	114
50	1.6×10^4	0.50	67
100	3.25×10^4	0.55	52
200	6.5×10^4	0.60	40

and the local mass transfer coefficient k_d by expressions of the type [17]:

$$Sh = \frac{k_d x}{D} = A\left(ReSc\frac{d_e}{x}\right)^{1/3} \qquad (3)$$

where the constant parameter A depends on the ratio between the channel width and its thickness h.

By combining Equations 1, 2 and 3, it follows that k_d varies linearly with k'; the theoretical expression is reported in Fig. 11. The agreement with the experimental results is quite satisfactory and the deviations observed may be explained by the fact that the separator is not a perfectly rigid wall and that some small differences exist in the microelectrode area.

2. In the presence of gas bubbles ($I_g \neq 0$), the relation between k_d and k' is no longer linear and by means of a regression analysis it was found that k_d varies linearly with $k'^{3/2}$ (see Fig. 11). This is quite similar to what occurs in natural turbulence. Indeed [18] the turbulent flux τ_x of the x component of the momentum, also called the turbulent shear stress, and the turbulent mass flux N_M near the interface, are given by:

$$\tau_x = -(\nu + \nu_t)\rho\frac{\partial \bar{v}_x}{\partial y} \simeq \tau_e \qquad (4a)$$

and

$$N_M = -(D + D_t)\frac{\partial \bar{C}}{\partial y} \simeq (N_M)_e = k_d C_0 \qquad (4b)$$

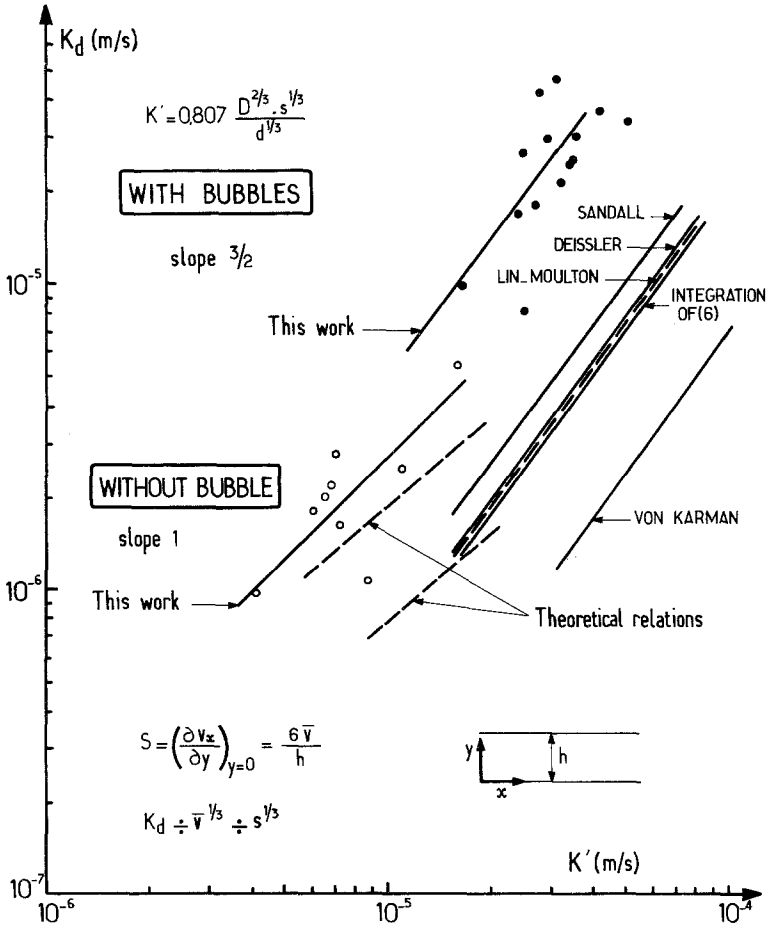

Fig. 11. Experimental variations of k_d (mass transfer coefficient) with k' (momentum transfer coefficient) with and without gas bubbles. Comparison with different correlations in natural turbulence.

where ν_t and D_t are the turbulent diffusivities of momentum and mass transfer respectively.

In the theories of turbulent mass and momentum transfer near a solid wall, it is frequent to introduce dimensionless variables defined as follows [19]:

$$\text{*Shear stress velocity: } v^* = \left(\frac{\tau}{\rho}\right)^{1/2} = \left(\frac{s}{\nu}\right)^{1/2}$$

$$\text{*Adimensional length: } y^+ = \frac{y v^*}{\nu} \qquad (5)$$

$$\text{*Normalized density: } v^+ = \frac{\bar{v}_x}{v^*}$$

By combining Equations 4 and 5, the following equation is derived for k_d [18]:

$$k_d = v^* / \int_0^\infty \left[\frac{dy^+}{Sc^{-1} + \left(\frac{\partial v^+}{\partial y^+}\right)^{-1} - 1} \right] \qquad (6)$$

or

$$k_d = v^* f(Sc) \qquad (7)$$

Furthermore v^*, which is directly proportional to $s^{1/2}$ (cf. Equation 5), can be calculated from k' (proportional to $s^{1/3}$) through:

$$v^* = \alpha k'^{3/2} \qquad (8)$$

with

$$\alpha = 1.38 \frac{\nu^{1/2} d^{1/2}}{D}$$

Combining Equations 7 and 8 leads to:

$$k_d = \alpha k'^{3/2} f(Sc) \qquad (9)$$

This model based on an analogy between both transfer mechanisms at the wall shows that k_d varies linearly with $k'^{3/2}$ and is in good agreement with the experimental results of Fig. 11 in so far as the value 3/2 of the slope is concerned.

In natural turbulence, many equations have been proposed for the generalized velocity profile $v^+ = f(y^+)$ (see for example [20] and [19]). In laminar flow and at high Schmidt numbers, the concentration boundary layer is much thinner than the hydrodynamic one and a good approximation for Equations 6 or 7 is the following (by taking $y^+ = 20$ as an arbitrary upper limit [18]):

$$k_d = 5.8 \times 10^{-2} Sc^{-2/3} v^* \qquad (10)$$

(valid for $Sc > 100$)

Other expressions for k_d based on the same analogy have been proposed in the literature and some of them are reported in Table 2; they generally relate the Stanton number, $St = k_d/\bar{v}$ to the friction factor:

$$f/2 = \frac{\tau}{\rho \bar{v}^2} = \left(\frac{v^*}{\bar{v}}\right)^2 \qquad (11)$$

The Von Karman analogy [21] assumes the existence of three zones in the generalized velocity profile (see Table 2).

Taking the limit of the Stanton number for high values of Sc leads to

$$k_d = \frac{v^*}{5\,Sc} \qquad (12)$$

However, the precision of this model decreases when Sc increases. Lin *et al.* [22] have proposed a model taking into account the presence of small eddies in the laminar sublayer. They used a power law for the turbulent momentum diffusivity near the wall:

$$\frac{\nu_t}{\nu} = \left(\frac{y^+}{14.5}\right)^3 \qquad (13)$$

and by integration obtained an expression for St, which for high Schmidt numbers gives:

$$k_d = \frac{v^*}{1702} \qquad (14)$$

Finally two other similar models have been derived by Sandall *et al.* [23] and Deissler [24]: in the latter, the existence of four zones has been defined for the generalized velocity profile.

Fig. 11 reports the corresponding correlations and compares them with the experimental results in the presence of electrogenerated gas bubbles (artificial turbulence). The agreement between the different models of natural turbulence is good except for the Von Karman analogy, which is not valid for high Sc numbers. With the gas, the mass transfer coefficient is an order of magnitude higher ($\simeq \times 9$) for a given value of k', i.e. of the fluid shear stress at the electrode.

Therefore, the analogy between turbulent mass and momentum transfer, which leads to a linear relationship between k_d and v^*, still remains valid, but the analytical form of the generalized velocity profile $v^+ = f(y^+)$ is modified compared to that prevailing in natural turbulence. Consequently, electrogeneration of gas bubbles represents an efficient means of increasing the mass transfer rate from an energetical point of view (s or the shear

Table 2.

von Karman 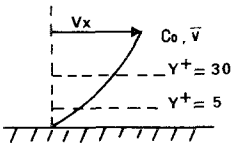 	$St = \dfrac{Kd}{\bar{v}} = \dfrac{f/2}{1 + 5(f/2)^{1/2}\{Sc - 1 + \ln[1 + \frac{5}{6}(Sc-1)]\}}$ High Schmidt number $K_d = v^*/5Sc$ $f/2 = \dfrac{v^{*2}}{\bar{v}^2}$
Lin Moulton Putnam (Eddies in the sublayer) $\dfrac{\nu_t}{\nu} = \left(\dfrac{y^+}{14.5}\right)^3$ for $y^+ < 5$	$St = \dfrac{f/2}{1 + (f/2)^{1/2} F(Sc)}$ $Sc \simeq 10^3$ $K_d = \dfrac{v^*}{1702}$
Sandall (Valid for high *Sc*)	$\dfrac{St}{(f/2)^{1/2}} = \left\{\begin{matrix} 12.48Sc^{2/3} - 7.85Sc^{1/3} + 3.61 \ln Sc \\ + 5.8 + 2.78 \ln\left(\dfrac{Re(f/2)^{1/2}}{90}\right) \end{matrix}\right\}^{-1}$ $Sc \simeq 10^3$ $K_d = \dfrac{v^*}{1200}$
Integration of Equation 6 (High *Sc*)	$K_d = \dfrac{v^* Sc^{-2/3}}{17.24}$

stress are related to the fluid pressure drop through the cell).

5. Conclusions

The electrochemical technique for simultaneously measuring the local mass transfer coefficient and fluid shear stress at a wall was found to be very useful for understanding the mechanism of mass transfer enhancement in the presence of electrogenerated gas bubbles. The well-known analogy relating both transfer in systems involving natural turbulence has been successfully tested here.

A more precise analysis should be derived by considering the effect of the Schmidt number experimentally and by extending the results to a higher range of electrogeneration rate i_g.

References

[1] Gh. Barthole, A. Storck, A. Laurent and J. C. Charpentier, *Int. Eng. Chem., Process Des. Dev.* **19** (1980) 514.

[2] *Idem, Entropie* **93** (1980) 30.

[3] *Idem, Int. Chem. Eng.* **22** (1982) 244.

[4] N. Ibl and J. Venczel, *Metalloberfläche* **24** (1970) 365.

[5] I. Rousar and V. Cezner, *Electrochim. Acta* **20** (1975) 289.

[6] K. Stephan and H. Vogt, *ibid.* **24** (1979) 11.

[7] L. J. J. Janssen and J. G. Hoogland, *ibid.* **18** (1973) 543.

[8] L. J. J. Janssen, *ibid.* **23** (1978) 81.

[9] *Idem, ibid.* **24** (1979) 693.

[10] A. Storck, Thesis, Nancy (1976).

[11] A. Storck and F. Coeuret, *Electrochim. Acta,* **22** (1977) 1155.

[12] A. Storck and D. Hutin, *ibid.* **26** (1981) 127.

[13] M. G. Fouad and G. H. Sedahmed, *ibid.* **17** (1972) 665.

[14] C. I. Elsner and S. L. Marchiano, *J. Appl. Electrochem.* **12** (1982) 735.

[15] G. Cognet, M. Lebouche and M. Souhar, *AIChE J.* **30** (1984) 338.

[16] L. Rosenhead, 'Laminar Boundary Layers', Oxford University Press, Oxford (1963).

[17] D. J. Pickett, 'Electrochemical Reactor Design', Elsevier, New York (1977) Chap. 4, pp. 125–134.

[18] N. Ibl, in 'Comprehensive Treatise of Electrochemistry', Vol. 6, Plenum Press, New York (1983) Chap. 3.

[19] F. Coeuret and A. Storck, 'Eléments de Génie Electrochimique', Technique et Documentation, Lavoisier, Paris (1984).
[20] D. T. Wasan and C. R. Wilke, *Int. J. Heat Mass Transfer* 7 (1964) 87.
[21] E. R. G. Eckert and J. F. Gross, 'Introduction to Heat and Mass Transfer' McGraw Hill, New York (1963).
[22] C. S. Lin, E. B. Denton, H. L. Gaskill and G. L. Putnam, *Ind. Eng. Chem.* **43** (1951) 2136.
[23] O. C. Sandall, O. T. Hanna and P. R. Mazet, *Can. J. Chem. Eng.* **58** (1980) 443.
[24] R. G. Deissler, NACA Report 1210 (1955).